Hippocampal GFAP-positive astrocyte responses to amyloid and tau pathologies

Marco Antônio De Bastiani, PhD[1*], Bruna Bellaver, PhD[1,2*], Wagner S. Brum[1,3], Debora G. Souza, PhD[1], Pamela C. L. Ferreira, PhD[2], Andreia S. Rocha, MA[1], Guilherme Povala, MA[1], João Pedro Ferrari-Souza[1,2], Andrea L. Benedet, PhD[3], Nicholas J. Ashton, PhD[3,4,5,6], Thomas K. Karikari, PhD[2,3,4], Henrik Zetterberg, MD. PhD[3,4,7,8,9], Kaj Blennow, MD. PhD[3,4], Pedro Rosa-Neto, MD. PhD[10], Tharick A. Pascoal, MD. PhD[2], Eduardo R. Zimmer, PhD[1,11,12] , for the Alzheimer's Disease Neuroimaging Initiative

*Both authors contributed equally to this article

[1]Graduate Program in Biological Sciences: Biochemistry, Universidade Federal do Rio Grande do Sul, Porto Alegre, RS, Brazil.

[2]Department of Psychiatry, University of Pittsburgh, Pittsburgh, PA, USA.

[3]Department of Psychiatry and Neurochemistry, The Sahlgrenska Academy at the University of Gothenburg, Mölndal, Sweden.

[4]Clinical Neurochemistry Laboratory, Sahlgrenska University Hospital, Gothenburg, Sweden.

[5]Wallenberg Centre for Molecular and Translational Medicine, University of Gothenburg, Gothenburg, Sweden.

[6]Department of Old Age Psychiatry, Institute of Psychiatry, Psychology & Neuroscience, King's College London, London, UK.

[7]Department of Neurodegenerative Disease, UCL Queen Square Institute of Neurology, London, UK.

[8]UK Dementia Research Institute at UCL, London, UK.

[9]Hong Kong Center for Neurodegenerative Diseases, Hong Kong, China.

[10]Translational Neuroimaging Laboratory (TNL), McGill Center for Studies in Aging (MCSA), Douglas Mental Health University Institute, Departments of Neurology and Neurosurgery, Psychiatry, and Pharmacology, McGill University, Montreal, Canada.

[11]Department of Pharmacology, Universidade Federal do Rio Grande do Sul, Porto Alegre, RS, Brazil.

[12]Graduate Program in Biological Sciences: Pharmacology and Therapeutics, Universidade Federal do Rio Grande do Sul, Porto Alegre, RS, Brazil.

Corresponding author:

Eduardo R. Zimmer, PhD (E.R. Zimmer)

Department of Pharmacology, Universidade Federal do Rio Grande do Sul (UFRGS)

2500 Ramiro Barcelos street, 90035-003, Porto Alegre, RS, Brazil

Email address: eduardo.zimmer@ufrgs.br

Telephone: +55 51 33085558

Fax: +55 51 33085544

Website: www.zimmer-lab.org

Word count: 4224

Abstract

Introduction: In Alzheimer's disease clinical research, glial fibrillary acidic protein (GFAP) released into the cerebrospinal fluid and blood is widely measured and perceived as a biomarker of reactive astrogliosis. However, it was demonstrated that GFAP levels differ in individuals presenting with amyloid-β (Aβ) or tau pathology. The molecular underpinnings behind this specificity are unexplored. Here we investigated biomarker and transcriptomic associations of GFAP-positive astrocytes with Aβ and tau pathologies in humans and mouse models.

Methods: We studied 90 individuals with plasma GFAP, Aβ- and Tau-PET to investigate the association between biomarkers. Then, transcriptomic analysis in hippocampal GFAP-positive astrocytes isolated from mouse models presenting Aβ (PS2APP) or tau (P301S) pathologies was applied to explore differentially expressed genes (DEGs), Gene Ontology processes, and protein-protein interaction networks associated with each phenotype.

Results: In humans, we found that plasma GFAP associates with Aβ but not tau pathology. Unveiling the unique nature of GFAP-positive astrocytic responses to Aβ or tau pathology, mouse transcriptomics showed scarce overlap of DEGs between the Aβ and tau mouse models, While Aβ GFAP-positive astrocytes were overrepresented with genes associated with proteostasis and exocytosis-related processes, tau hippocampal GFAP-positive astrocytes presented greater abnormalities in functions related to DNA/RNA processing and cytoskeleton dynamics.

Conclusion: Our results offer insights into Aβ- and tau-driven specific signatures in GFAP-positive astrocytes. Characterizing how different underlying pathologies distinctly influence astrocyte responses is critical for the biological interpretation of astrocyte-related biomarker and suggests the need to develop context-specific astrocyte targets to study AD.

Funding: This study was supported by Instituto Serrapilheira, Alzheimer's Association, CAPES, CNPq and FAPERGS.

Keywords: biomarker, GFAP, amyloidosis, tau pathology, Alzheimer's disease

1. Introduction

Astrocytes are the main homeostatic cells of the brain, which are involved in most aspects of brain physiology. For a long time, the response of astrocytes to brain injury – a process collectively called astrocyte reactivity – was considered an almost universal phenomenon. Nowadays, there is a consensus that glial responses are rather complex, heterogeneous, and context-specific [1-3]. In this sense, astrocytes are likely decisive contributors to Alzheimer's disease (AD) onset and progression; however, the molecular underpinnings are still poorly understood. Furthermore, transcriptomics analysis in *postmortem* AD brains demonstrated highly variable intra-cohort astrocyte molecular signatures in individuals with the same clinical diagnosis, indicating that specific aspects of AD pathophysiology might be triggering different astrocyte phenotypes [4]. In this context, Jiwaji and colleagues started uncovering the heterogeneity of astrocyte reactivity facing Aβ and tau pathologies, the neuropathological hallmarks of AD [5].

Astrocyte biomarkers are reported to be consistently increased in cerebrospinal fluid (CSF) and blood of AD patients compared to cognitively unimpaired (CU) individuals [6, 7]. Although it is known that astrocyte reactivity cannot be measured by one single marker, clinical research commonly relies on the measurement of glial fibrillary acidic protein (GFAP) concentration in CSF or blood as a proxy of astrocyte reactivity. It was recently demonstrated that plasma GFAP levels are more associated with the Aβ burden than tau pathology in AD [8, 9] – an association that was found to be more robust in blood than in CSF. On the other hand, increased GFAP levels were already identified in primarily tau pathologies as in frontotemporal dementia [10-12]. In this sense, uncovering the phenotypes acquired by GFAP-positive astrocytes under Aβ or tau influence might directly impact clinical research by improving the biological interpretation of clinical biomarkers used in AD.

In this study, we investigated GFAP associations with Aβ and tau pathologies in individuals across aging and AD spectrum. Furthermore, we investigated the molecular signatures of GFAP-positive astrocytes driven by Aβ or tau, comparing the hippocampal transcriptomic profile of astrocytes from animal models of amyloidosis (PS2APP mice) and tau pathology (P301S mice). Differentially expressed genes (DEGs), protein-protein networks, and functional enrichment analysis of Gene Ontology (GO) terms were performed to identify biological differences and similarities between the phenotypes acquired by these astrocytes. The molecular characterization of astrocyte responses to Aβ and tau pathology may pave the way for a better understanding of the GFAP biological interpretation in AD.

2. Methods

2.1. Human Cohort

Data used in the preparation of this article were obtained from the Alzheimer's Disease Neuroimaging Initiative (ADNI) database, phases GO and 2. ADNI was launched in 2003 as a public-private partnership, led by Principal Investigator Michael W. Weiner, MD. The primary goal of ADNI has been to test whether serial magnetic resonance imaging (MRI), PET, other biological markers, and clinical and neuropsychological assessments can be combined to measure the progression of mild cognitive impairment (MCI) and early AD. ADNI study was conducted according to Good Clinical Practice guidelines, US 21CFR Part 50 – Protection of Human Subjects, and Part 56 – Institutional Review Boards, and pursuant to state and federal HIPAA regulations and was approved by the Institutional Review Board of each participating site (adni.loni.usc.edu). Written informed consent for the study was obtained from all participants and/or authorized representatives

Based on biomarker availability, 90 participants were included [CU: n = 39; cognitively impaired (CI; mild cognitive impairment (MCI) or AD dementia): n = 51] from the ADNI database. All participants had available measurements of plasma GFAP and positron emission tomography (PET) data for [^{18}F]-florbetapir (Aβ-PET) and [^{18}F]-flortaucipir (Tau-PET), within a maximum 2.5-year time interval between scan and plasma collection. Plasma GFAP was measured with Simoa Neurology 4-Plex (#103670, Quanterix). For Aβ-PET data analysis, as recommended for cross-sectional analyses [13], the global cortical composite standardized uptake value ratio (SUVr) normalized by the whole cerebellum was used. When applicable, global Aβ-PET cortical composite was used to dichotomize participants into Aβ-negative (A-) and Aβ-positive (A+) based on the widely validated ADNI cutoff of >1.11 [13]. For tau-PET, we assessed the temporal meta-ROI values and the cutoff for tau-PET positivity of 1.23 was used [14]. Baseline characteristics were summarized with descriptive statistics. Pearson correlation was applied to assess associations between biomarkers, and statistical significance was set to $\alpha = 0.05$ (FDR-adjusted).

2.2. RNA-seq Data Acquisition and Differential Expression Analysis

Expression profiling by high throughput sequencing studies of mice hippocampus GFAP-positive astrocytes were obtained from the NCBI Gene Expression Omnibus (GEO) (https://www.ncbi.nlm.nih.gov/geo). The first study (GSE129770) contains data from 5

PS2APP and 5 wild-type (WT) mice (11.5-months old); the second study (GSE129797) contains data from 5 Tau P301S and 5 WT mice (6-months old)[15]. First, raw RNA-seq data from both studies was downloaded using the SRA Toolkit (https://github.com/ncbi/sra-tools). Afterwards, transcript alignment was performed using Salmon (v1.3.0) [16], mapped to a reference genome with the index derived from *Mus musculus* GRCm38 Ensembl build. Aligned reads were summarized using tximport (v1.12.3) [17] and genes with mean count < 10 were filtered out. Finally, processed expression data from both hippocampus astrocyte studies was analyzed with the DESeq2 (v1.28.1) [18] method for differential expression evaluation of either PS2APP or Tau P301S mutations *versus* respective WT mice. Genes with FDR adjusted p-value < 0.1 were considered as DEGs for further analyses. Venn diagrams were constructed using the VennDiagram package (v1.6.20).

2.3. Functional Enrichment Analysis and Network

Gene Ontology (GO) enrichment analysis of DEGs previously obtained for both studies was implemented using the clusterProfiler (v3.16.1) package [19]. The significantly enriched terms from biological process (BP), cellular component (CC) and molecular function (MF) sub-ontologies were used to build networks employing the RedeR (v1.36.0) and GOplot (v1.0.2) packages [20, 21]. In this network, GO terms are mapped to nodes and edges represent the proportion of gene overlap (Jaccard Coefficient > 0.15) between all pairs of terms.

2.4. Protein-Protein Interaction Networks and Circos Plots

We used the *Search Tool for the Retrieval of Interacting Genes/Proteins* (STRING) Consortium to build protein-protein interaction (PPI) networks with the DEGs for both datasets. STRING is a biological database and web resource of known and predicted protein–protein interactions which contains information from numerous sources, including experimental data, computational prediction methods and public text collections. The construction of the networks was implemented in R using the STRINGdb (v2.0.2), RedeR (v1.36.0) and igraph (v1.2.6) packages [20, 22]. Final network was filtered to retain only gene connections with STRING combined confidence interaction scores > 0.7. For each PPI network, genes observed in GO terms significantly enriched were manually curated and categorized. These functional categorizations were used to create circos plots showing category linkages and link proportions in PS2APP and Tau P301S networks. The plots were built using the circlize package (v0.4.13) [23].

3. Results

3.1. Plasma GFAP differently associates with biomarkers of AD pathology

Table 1 shows demographic information of the 90 individuals (39 CU and 51 CI) assessed. Correlations between GFAP and other known biomarkers of AD pathology and neurodegeneration showed that GFAP negatively correlated with CSF Aβ42/40, but no significant associations were observed with p-Tau181 (**Supplemental Fig. 1**). We then further investigated associations between Aβ- and Tau-PET with plasma GFAP levels in individuals across aging and the AD continuum. Linear regressions using composite brain regions revealed that both Aβ- and Tau-PET significantly associated with plasma GFAP (**Fig. 1A, C**). However, when individuals were stratified by their Aβ status (A- and A+), we observed that the association between Aβ- and Tau-PET with plasma GFAP remains significant only in A+ individuals (**Fig. 1B, D**).

Furthermore, we evaluated whether GFAP levels are associated with changes in Tau-PET, to further assess how this effect would be affected by including Aβ-PET as a covariate. We built models including either (i) Braak III-IV or (ii) Braak V-VI SUVr as the outcomes, with two predictor schemes, plasma GFAP alone or plasma GFAP and Aβ-PET global SUVr, resulting in four models. For Braak III-IV SUVr as the outcome, increases in plasma GFAP were associated with increases in Tau-PET (β-estimate: 0.054; $t = 3.68$; $p < 0.001$). When including plasma GFAP and Aβ-PET as predictors, plasma GFAP was no longer associated with increases in Tau-PET (β-estimate: 0.019; $t = 1.35$; $p = 0.18$). For Braak V-VI as the outcome, the same was observed. In the univariate model, increases in plasma GFAP were associated with increases in Tau-PET (β-estimate: 0.031; $t = 2.43$; $p = 0.02$). When Aβ-PET SUVr was also added as predictor, plasma GFAP was no longer associated with increases in Tau-PET (β-estimate: 0.0059; $t = 0.46$; $p = 0.65$). Our results corroborate previous studies in other cohorts [8, 9], evidencing the specificity of plasma GFAP association with Aβ, but not tau pathology in AD.

3.2. GFAP-positive astrocytes affected either by Aβ or tau pathology present a scarce overlap of DEGs

To better understand the biological underpinnings of GFAP association with Aβ pathology, we compared GFAP-positive astrocytes isolated from Aβ and tau mouse models.

The amyloidosis model (PS2APP) presented 95 downregulated genes (adjusted p-value < 0.1) compared to WT mice (**Fig. 2A**). Log fold change values ranged from -2.9365 to -0.4204. The most significantly downregulated gene was Aquaporin 11 (Aqp11), which encodes a water channel protein that also facilitates the transport of glycerol and hydrogen peroxide across membranes. In addition, 200 upregulated genes were also found compared to WT mice (adjusted p-value < 0.1) comprising log fold change values ranging from 0.4308 to 4.9284. The most significant upregulated gene was PTPN6, which encodes the Protein Tyrosine Phosphatase Non-receptor Type 6, also known as Src homology region 2 domain-containing phosphatase-1 (SHP-1), a tyrosine phosphatase enzyme. The Tau model (P301S) presented 178 statistically significant downregulated genes compared to WT mice (**Fig. 2B**). The expression of Insulin-1 (Ins1) and Insulin-2 (Ins2) were mostly impacted. These genes encode the hormone insulin, and may play a role in growth, differentiation and glucose metabolism in the brain. The other downregulated genes ranged between -4.098 to -0.507 log fold change and are related to different pathways. In parallel, 427 statistically significant upregulated genes were found in Tau P301S compared to WT mice. The log fold change values ranged from 0.5216 to 4.212. The most significant upregulated gene identified was Retrotransposon Gag Like 8B (Rtl8b), also known as Mart, considered a neofunctionalized retrotransposon gene. Interestingly, only 30 DEGs overlapped among astrocytes from these two mouse models, revealing Aβ and tau drive specific astrocyte molecular remodeling (**Fig. 2C**). Results of differential expression analysis for both animal models are presented in **Supplemental Table 1**.

3.3. Aβ and tau pathology promote the enrichment of distinct functional categories in GFAP-positive astrocytes

The PPI analysis showed a network containing 70 altered nodes in the PS2APP hippocampal astrocytes dataset. The average node degree was 3.285 and the number of edges was 115 (expected: 74). The average local clustering coefficient was 0.521, while the global clustering coefficient was 0.21. Based on the connectivity degree, Uba52, Ubc, Ccnh, Arrb2, and Gng12 were the top 5 hub proteins. The results were plotted as a PPI network (**Fig. 3A**). Circos plot (**Fig. 3B**) indicates the altered protein interconnectivity in the network based on their functional categories, with "Proteostasis" being the leading functional alteration in PS2APP astrocytes.

The PPI data analysis showed a different profile of the gene network in the Tau P301S model compared to the PS2APP. PPI analysis of the Tau P301S hippocampal astrocytes showed 204 altered nodes. The average node degree was 4.137 and the number of edges was 422 (expected: 373). The average local clustering coefficient was 0.551, and the global clustering coefficient was 0.5. Based on the connectivity degree, Stat1, Usp18, Irf7, Pik3ca, and Cxcl10 were among the top 5 hub proteins. The results were plotted as a PPI network and protein nodes were colored according to their functional category (**Fig. 3C**). Circos plot (**Fig. 3D**) indicates the interconnectivity of the altered proteins based on their functional categories, being "DNA/RNA processing", “Inflammation” and “Cytoskeleton” the leading functional alterations. The modulation of gene expression for both networks can be visualized in **Supplemental Fig. 2**.

3.4. Aβ and tau pathologies drive GFAP-positive astrocytes changes in Gene Ontology biological domains

The functional enrichment analysis revealed 36 GO terms enriched with DEGs altered in the PS2APP mice compared to its WT controls (**Supplemental Table 2**). We found 14 BP, 8 CC and 14 MF in the analysis. Fig. 4A shows the network of GO terms enriched, in which we mapped the degree of connectivity for each term in the node sizes and the pairwise gene overlap (Jaccard coefficient) between terms in the edges. We noted that "exocytosis", "exocytic process", "protein localization to cell periphery", "protein localization to plasma membrane" and "voltage−gated cation channel activity" are the most connected terms in the network (Fig. 4B). On the other hand, the most significantly enriched terms are shown in **Fig. 4C**, which include processes such as “protein localization to cell periphery and plasma membrane”, “interleukin−6 production and regulation”, “interleukin−6 production and regulation”, “exocytosis” and “neuron death”.

For the comparison of the Tau P301S mice *versus* WT controls, the functional enrichment analysis using DEGs revealed 95 terms (**Supplemental Table 2**), which include 56 BP, 25 CC and 14 MF enriched terms. The GO network for Tau P301S shows that the most connected terms are related to cytoskeleton dynamics such as “actin filament binding and organization” and “cell leading edge” (**Fig. 4D-E**). Among the most significantly enriched terms, we found terms such as “learning”, “cognition”, and “small GTPase mediated signal transduction” (**Fig. 4F**). Results of the functional enrichment analysis for both animal models are presented in **Supplemental Table 2**.

4. Discussion

Here, we evaluated the association of plasma GFAP levels with Aβ and tau pathologies in CU and CI individuals. We demonstrated that GFAP independently associates with Aβ, but not with tau pathology. To understand the impact of Aβ and tau pathology separately in GFAP-positive astrocyte phenotypes, we explored the molecular features of astrocytes isolated from the hippocampus of two AD mouse models (PS2APP and Tau P301S). Overall, we observed a limited overlap of DEGs between the Aβ and tau mouse models, indicating the unique nature of GFAP-positive astrocytic responses to different aspects of AD pathology. The findings presented in this study allowed the identification of functional categories and biological processes that are a distinctive response to Aβ or tau burden.

Astrocyte biomarkers have been increasingly investigated in AD, and they have already proved to be consistently altered in AD patients [6]. However, the production and consequent release of GFAP by astrocytes in response to AD pathological events seem heterogeneous. Specifically, while GFAP seems to be more associated with Aβ burden [8, 9, 24] it does not correlate with tau when corrected for Aβ pathology. On the other hand, studies investigating another astrocyte biomarker – the chitinase-3-like protein 1 (YKL-40) – demonstrated that YKL-40 seems to be more associated with tau pathology [25-27]. These findings highlight the importance of understanding how astrocytes react to specific aspects of AD pathology.

A large portion of the current knowledge regarding the astrocytic responses to AD pathology was obtained from *postmortem* studies in patients with dementia. At this point, the human brain is usually affected by several pathological components of AD simultaneously, hampering the understanding of the exact role each one is playing in the disease. The use of animal models provides a unique opportunity to explore isolated pathological features of AD and better comprehend its heterogeneous aspects. Our comparison of GFAP-positive astrocytes from animal models of Aβ and tau pathologies evidenced a scarce overlap of genes between these two transgenic lines. At the moment, only a few studies in the literature aimed at stratifying the unique astrocyte signatures triggered by Aβ or tau [5, 15]. Wu and colleagues specifically focused on the complement C1q cascade, demonstrating that tau pathology is enough to activate the classical complement pathway [15]. In a broader approach, Jiwaji et al. demonstrated a significant overlap of DEGs between astrocytes from

Aβ and tau pathology. Our study and the one by Jiwaji and colleagues are highly complementary since present different methodologies. More specifically, studies used different brain regions (hippocampus *vs* whole cortex and spinal cord) and cell-sorting protocols that isolated distinct astrocyte populations (GFAP-positive astrocytes *vs* pan astrocytes) [5]. Despite the exciting insights provided by these recent studies, the understanding of astrocyte heterogeneity in AD is still in its early days, and further studies exploring region-specificity and disease/pathology stages are still needed.

Differential expression analysis in the PS2APP GFAP-positive astrocytes revealed that Aqp11 appeared as the most downregulated gene. In humans, AQP11 co-localizes to the endoplasmic reticulum (ER) and mitochondrial-associated membrane (MAM) to facilitate the transport of hydrogen peroxide [28, 29]. In the ER, AQP11-mediated peroxide transit seems to prevent toxicity during protein folding [29]. The downregulation of this peroxiporin in our analysis suggests the presence of ER stress in PS2APP GFAP-positive astrocytes. Additionally, as APP is synthesized in the ER, alterations in MAMs and ER stress are emerging as important pathological mechanisms of AD and interesting therapeutic targets to modify protein misfolding and synaptic failure [30-32]. Furthermore, the upregulation of ubiquitin-related genes (Uba52, Ubc) may indicate compensatory attempts to mitigate the results of ER stress. Ubiquitination is a major post-translational modification responsible for many actions in the cells, including protein degradation, kinases modification and regulation of signaling pathways. The PPI network analysis also evidenced that ER stress is an important alteration in PS2APP hippocampal astrocytes. In specific, the most connected proteins of this network (Ubc and Uba52) were associated with proteostasis. This functional category showed high linkage with others, especially intracellular trafficking, and DNA/RNA processing. Indeed, a recent systematic review of AD neuropathological literature showed proteostasis among the most consistent functional alterations of the disease, however its specificity for Aβ pathology was not demonstrated [33]. Furthermore, Tau P301S astrocytes PPI shows more genes associated with DNA/RNA processing function than PS2APP astrocytes. Site-specific phosphorylation regulates tau and, since nuclear tau protects the DNA [34, 35], its dysfunction can alter the chromatin landscape in pathological contexts [36, 37]. The DNA/RNA processing function contained Myc, Yy1, histone deacetylases, among other genes associated with DNA-binding and epigenetic GO terms. Although astrocyte and neuron chromatin dysfunction have been reported [38], it is not clear how tau-induced astrocyte dysfunction and associated chromatin alterations may influence other pathological features of AD.

The differential expression analysis of the Tau P301S astrocytes revealed dysregulation of insulin-related genes and downstream signaling kinases. Indeed, Ins1/2 and Pi3kca, proteins directly involved in regulating energetic brain metabolism, were highly connected and downregulated nodes in the Tau P301S PPI network. In this context, several pathophysiological links have been demonstrated between AD and metabolic disorders such as type 2 diabetes, obesity, and metabolic syndrome in humans and animal models [39-42]. Furthermore, it has been demonstrated that when insulin signaling is impaired in astrocytes, brain glucose uptake become less efficient, impairing CNS control of glucose homeostasis [42, 43]. As insulin plays a central role in regulating tau phosphorylation in the brain, deficiencies in insulin signaling could exacerbate neurodegeneration by promoting tau hyperphosphorylation in neurons [44, 45]. Despite *in vitro* studies demonstrating that insulin signaling in astrocytes is affected by Aβ exposure [46, 47], our findings showed that it does not seem to play a significant role in an animal model presenting Aβ deposition without tau pathology. In fact, the strong link between tau pathology and changes in insulin signaling has been reported in *postmortem* AD and other human tauopathies [48].

Interpreting transcriptomic changes at the pathway level is more consistent than single gene analysis, and it has the potential to offer insights into the biological processes disturbed in AD. Our functional enrichment analysis identified multiple biological processes driven by each specific aspect of AD pathology. Exocytosis-related processes are among the most significant biological processes enriched in the PS2APP mice. Interestingly, impaired exocytosis was already reported in AD, specifically in brain regions susceptible to neurodegeneration [49]. Corroborating, previous studies have been linking impaired exocytosis in the brain [50], and specifically in astrocytes [51], as a result of Aβ exposure, which might compromise proper neurotransmitter release. Astrocytes play a pivotal role in maintaining synaptic strength via vesicular exocytosis of glutamate and ATP [52]. Interestingly, our PPI analysis evidenced neurotransmission as one of the main functional categories disturbed in the PS2APP, but not in the Tau 301S astrocytes. In this sense, abnormalities in astrocyte exocytic activity might represent an underexplored aspect of AD pathology.

Neuroinflammation is now a well-recognized and active process detectable in the early stages of AD. A recent study using the [^{11}C]PRB28 tracer revealed that inflammation and tau propagate jointly in the brain of AD patients in an Aβ-dependent manner [53]. We observed that abnormalities in inflammation-related processes were prominent in both Tau 301S and PS2APP astrocytes. Accordingly, it was previously demonstrated that Aβ and tau

are able to independently trigger an inflammatory response that contributes to neurodegeneration in mice [54, 55], however, the presence of both pathologies simultaneously potentiates this process [54]. Additionally, the release of inflammatory mediators by astrocytes seems to be essential for Aβ-induced tau phosphorylation in primary neurons [56]. Although microglia are the main players in the brain immune response, astrocytes also respond to CNS threats by releasing a range of cytokines that perpetuate the harmful environment in AD [57-59].

5. Conclusion

The recent advances in understanding the neuropathological features of AD revealed a high degree of complexity in the astrocytic response to this disease. Additionally, the rapid growth in the AD fluid biomarkers field demonstrated that this complexity is reflected outside the brain. Indeed, comprehending AD blood biomarkers biological interpretation is one of the filed greatest challenges. The paucity of overlap between Aβ- and tau-driven DEGs strikingly shows the specific nature of GFAP-positive astrocyte responses to core AD pathology. Our results revealed multiple astrocyte-related biological processes and potential functional alterations triggered by each aspect of AD pathophysiology. Thus, developing novel biomarkers that reliably reflect AD heterogeneity seems critical to determine AD pathology's underpinnings and consequently monitor the efficacy and target engagement of emerging anti-Aβ and anti-tau drugs and develop personalized treatment strategies.

DECLARATIONS

Ethics approval and consent to participate

Not applicable.

Availability of data and materials

Datasets used in this study can be accessed via NCBI GEO portal (https://www.ncbi.nlm.nih.gov/geo/). Further intermediate data and codes generated are available from the corresponding author upon request.

Competing interests

HZ has served at scientific advisory boards and/or as a consultant for Abbvie, Alector, Annexon, Artery Therapeutics, AZTherapies, CogRx, Denali, Eisai, Nervgen, Novo Nordisk, Pinteon Therapeutics, Red Abbey Labs, Passage Bio, Roche, Samumed, Siemens Healthineers, Triplet Therapeutics, and Wave, has given lectures in symposia sponsored by Cellectricon, Fujirebio, Alzecure, Biogen, and Roche, and is a co-founder of Brain Biomarker Solutions in Gothenburg AB (BBS), which is a part of the GU Ventures Incubator Program (outside submitted work). The other authors declare that they have no conflict of interest.

Funding

We would like to thank the funding agencies that supported this work. ERZ receives financial support from CNPq [460172/2014-0], PRONEX, FAPERGS/CNPq [16/2551-0000475-7], Brazilian National Institute of Science and Technology in Excitotoxicity and Neuroprotection [465671/2014-4], FAPERGS/MS/CNPq/SESRS–PPSUS [30786.434.24734.23112017], Instituto Serrapilheira [Serra-1912-31365], Alzheimer's Association [AARGD-21-850670]. MAB received financial support from CNPq [150293/2019-4]. BB receives financial support from CAPES [88887.336490/2019-00] and Alzheimer’s Association (AARFD-22-974627). PRN is funded by Fonds de Recherche du Québec – Santé (FRQS; Chercheur Boursier, PR-N and 2020-VICO-279314) and CIHR-CCNA Canadian Consortium of Neurodegeneration in Aging. TKK is funded by the Swedish Research Council (Vetenskåpradet; #2021-03244), the Alzheimer’s Association (#AARF-21-850325), the BrightFocus Foundation (#A2020812F), the International Society for Neurochemistry’s Career Development Grant, the Swedish Alzheimer Foundation (Alzheimerfonden; #AF-930627), the Swedish Brain Foundation (Hjärnfonden; #FO2020-0240), the Swedish Dementia Foundation (Demensförbundet), the

Swedish Parkinson Foundation (Parkinsonfonden), Gamla Tjänarinnor Foundation, the Aina (Ann) Wallströms and Mary-Ann Sjöbloms Foundation, the Agneta Prytz-Folkes & Gösta Folkes Foundation (#2020-00124), the Gun and Bertil Stohnes Foundation, and the Anna Lisa and Brother Björnsson's Foundation. HZ is a Wallenberg Scholar supported by grants from the Swedish Research Council (#2018-02532), the European Research Council (#681712), Swedish State Support for Clinical Research (#ALFGBG-720931), the Alzheimer Drug Discovery Foundation (ADDF), USA (#201809-2016862), the AD Strategic Fund and the Alzheimer's Association (#ADSF-21-831376-C, #ADSF-21-831381-C and #ADSF-21-831377-C), the Olav Thon Foundation, the Erling-Persson Family Foundation, Stiftelsen för Gamla Tjänarinnor, Hjärnfonden, Sweden (#FO2019-0228), the European Union's Horizon 2020 research and innovation programme under the Marie Skłodowska-Curie grant agreement No 860197 (MIRIADE), the European Union Joint Programme – Neurodegenerative Disease Research (JPND2021-00694), and the UK Dementia Research Institute at UCL (UKDRI-1003). TAP is supported by the Alzheimer's Association (grant AACSF-20-648075) and National Institute of Aging (grants R01AG075336, R01AG073267).

Author Contributions

MAB: conceptualization, data curation, formal analysis, data interpretation, figures, writing – original draft, and writing – review & editing.

BB: conceptualization, data curation, formal analysis, data interpretation, figures, writing – original draft, and writing – review & editing.

WSB: data curation, formal analysis, data interpretation, figures, writing – review & editing.

DGS: data curation, formal analysis, data interpretation, figures, writing – review & editing.

PCLF: data curation, formal analysis, data interpretation, figures, writing – review & editing.

ASR: data curation, formal analysis, data interpretation, figures, writing – review & editing.

GP: data curation, formal analysis, data interpretation, figures, writing – review & editing.

JPF-S: data interpretation, writing – review & editing.

ALB: writing – review & editing.

NJA: writing – review & editing.

TKK: writing – review & editing.

HZ: writing – review & editing.

KB: writing – review & editing.

PR-N: writing – review & editing.

TAP: writing – review & editing.

ERZ: conceptualization, data interpretation, funding acquisition, supervision, writing – original draft, and writing – review & editing.

References

1. Siracusa, R., R. Fusco, and S. Cuzzocrea, *Astrocytes: Role and Functions in Brain Pathologies.* Front Pharmacol, 2019. **10**: p. 1114.
2. Verkhratsky, A. and M. Nedergaard, *Physiology of Astroglia.* Physiol Rev, 2018. **98**(1): p. 239-389.
3. Escartin, C., et al., *Reactive astrocyte nomenclature, definitions, and future directions.* Nat Neurosci, 2021. **24**(3): p. 312-325.
4. Galea, E., et al., *Multi-transcriptomic analysis points to early organelle dysfunction in human astrocytes in Alzheimer's disease.* Neurobiol Dis, 2022. **166**: p. 105655.
5. Jiwaji, Z., et al., *Reactive astrocytes acquire neuroprotective as well as deleterious signatures in response to Tau and Aß pathology.* Nat Commun, 2022. **13**(1): p. 135.
6. Bellaver, B., et al., *Astrocyte Biomarkers in Alzheimer Disease: A Systematic Review and Meta-analysis.* Neurology, 2021.
7. Carter, S.F., et al., *Astrocyte Biomarkers in Alzheimer's Disease.* Trends Mol Med, 2019. **25**(2): p. 77-95.
8. Pereira, J.B., et al., *Plasma GFAP is an early marker of amyloid-β but not tau pathology in Alzheimer's disease.* Brain, 2021. **144**(11): p. 3505-3516.
9. Benedet, A.L., et al., *Differences Between Plasma and Cerebrospinal Fluid Glial Fibrillary Acidic Protein Levels Across the Alzheimer Disease Continuum.* JAMA Neurol, 2021. **78**(12): p. 1471-1483.
10. Katisko, K., et al., *GFAP as a biomarker in frontotemporal dementia and primary psychiatric disorders: diagnostic and prognostic performance.* J Neurol Neurosurg Psychiatry, 2021. **92**(12): p. 1305-1312.
11. Heller, C., et al., *Plasma glial fibrillary acidic protein is raised in progranulin-associated frontotemporal dementia.* J Neurol Neurosurg Psychiatry, 2020. **91**(3): p. 263-270.
12. Abu-Rumeileh, S., et al., *CSF biomarkers of neuroinflammation in distinct forms and subtypes of neurodegenerative dementia.* Alzheimers Res Ther, 2019. **12**(1): p. 2.
13. Landau, S.M., et al., *Comparing positron emission tomography imaging and cerebrospinal fluid measurements of β-amyloid.* Ann Neurol, 2013. **74**(6): p. 826-36.
14. Maass, A., et al., *Comparison of multiple tau-PET measures as biomarkers in aging and Alzheimer's disease.* Neuroimage, 2017. **157**: p. 448-463.
15. Wu, T., et al., *Complement C3 Is Activated in Human AD Brain and Is Required for Neurodegeneration in Mouse Models of Amyloidosis and Tauopathy.* Cell Rep, 2019. **28**(8): p. 2111-2123.e6.
16. Patro, R., et al., *Salmon provides fast and bias-aware quantification of transcript expression.* Nat Methods, 2017. **14**(4): p. 417-419.
17. Soneson, C., M.I. Love, and M.D. Robinson, *Differential analyses for RNA-seq: transcript-level estimates improve gene-level inferences.* F1000Res, 2015. **4**: p. 1521.
18. Walter, W., F. Sánchez-Cabo, and M. Ricote, *GOplot: an R package for visually combining expression data with functional analysis.* Bioinformatics, 2015. **31**(17): p. 2912-4.
19. Yu, G., et al., *clusterProfiler: an R package for comparing biological themes among gene clusters.* Omics, 2012. **16**(5): p. 284-7.

20. Castro, M.A., et al., *RedeR: R/Bioconductor package for representing modular structures, nested networks and multiple levels of hierarchical associations.* Genome Biol, 2012. **13**(4): p. R29.
21. Nelson, P.T., et al., *Correlation of Alzheimer disease neuropathologic changes with cognitive status: a review of the literature.* J Neuropathol Exp Neurol, 2012. **71**(5): p. 362-81.
22. Szklarczyk, D., et al., *STRING v11: protein-protein association networks with increased coverage, supporting functional discovery in genome-wide experimental datasets.* Nucleic Acids Res, 2019. **47**(D1): p. D607-d613.
23. Gu, Z., et al., *circlize Implements and enhances circular visualization in R.* Bioinformatics, 2014. **30**(19): p. 2811-2.
24. Chatterjee, P., et al., *Plasma glial fibrillary acidic protein is elevated in cognitively normal older adults at risk of Alzheimer's disease.* Transl Psychiatry, 2021. **11**(1): p. 27.
25. Alcolea, D., et al., *Amyloid precursor protein metabolism and inflammation markers in preclinical Alzheimer disease.* Neurology, 2015. **85**(7): p. 626-33.
26. Antonell, A., et al., *Cerebrospinal fluid level of YKL-40 protein in preclinical and prodromal Alzheimer's disease.* J Alzheimers Dis, 2014. **42**(3): p. 901-8.
27. Ferrari-Souza, J.P., et al., *Astrocyte biomarker signatures of amyloid-β and tau pathologies in Alzheimer's disease.* Mol Psychiatry, 2022.
28. Takahashi, S., et al., *The role of Cysteine 227 in subcellular localization, water permeability, and multimerization of aquaporin-11.* FEBS Open Bio, 2014. **4**: p. 315-20.
29. Bestetti, S., et al., *Human aquaporin-11 guarantees efficient transport of H(2)O(2) across the endoplasmic reticulum membrane.* Redox Biol, 2020. **28**: p. 101326.
30. Gerakis, Y. and C. Hetz, *Emerging roles of ER stress in the etiology and pathogenesis of Alzheimer's disease.* Febs j, 2018. **285**(6): p. 995-1011.
31. Fernandes, T., et al., *Structural and Functional Alterations in Mitochondria-Associated Membranes (MAMs) and in Mitochondria Activate Stress Response Mechanisms in an In Vitro Model of Alzheimer's Disease.* Biomedicines, 2021. **9**(8).
32. Gao, X. and Y. Xu, *Therapeutic Effects of Natural Compounds and Small Molecule Inhibitors Targeting Endoplasmic Reticulum Stress in Alzheimer's Disease.* Front Cell Dev Biol, 2021. **9**: p. 745011.
33. Viejo, L., et al., *Systematic review of human post-mortem immunohistochemical studies and bioinformatics analyses unveil the complexity of astrocyte reaction in Alzheimer's disease.* Neuropathol Appl Neurobiol, 2022. **48**(1): p. e12753.
34. Sultan, A., et al., *Nuclear tau, a key player in neuronal DNA protection.* J Biol Chem, 2011. **286**(6): p. 4566-75.
35. Rico, T., et al., *Tau Stabilizes Chromatin Compaction.* Front Cell Dev Biol, 2021. **9**: p. 740550.
36. Gil, L., et al., *Phospho-Tau and Chromatin Landscapes in Early and Late Alzheimer's Disease.* Int J Mol Sci, 2021. **22**(19).
37. Nativio, R., et al., *Publisher Correction: Dysregulation of the epigenetic landscape of normal aging in Alzheimer's disease.* Nat Neurosci, 2018. **21**(7): p. 1018.

38. Phipps, A.J., et al., *Neurofilament-labeled pyramidal neurons and astrocytes are deficient in DNA methylation marks in Alzheimer's disease.* Neurobiol Aging, 2016. **45**: p. 30-42.
39. Li, J., et al., *Effects of Diabetes Mellitus on Cognitive Decline in Patients with Alzheimer Disease: A Systematic Review.* Can J Diabetes, 2017. **41**(1): p. 114-119.
40. Sripetchwandee, J., N. Chattipakorn, and S.C. Chattipakorn, *Links Between Obesity-Induced Brain Insulin Resistance, Brain Mitochondrial Dysfunction, and Dementia.* Front Endocrinol (Lausanne), 2018. **9**: p. 496.
41. Diaz, A., et al., *Metabolic Syndrome Exacerbates the Recognition Memory Impairment and Oxidative-Inflammatory Response in Rats with an Intrahippocampal Injection of Amyloid Beta 1-42.* Oxid Med Cell Longev, 2018. **2018**: p. 1358057.
42. González-García, I., T. Gruber, and C. García-Cáceres, *Insulin action on astrocytes: From energy homeostasis to behaviour.* J Neuroendocrinol, 2021. **33**(4): p. e12953.
43. García-Cáceres, C., et al., *Astrocytic Insulin Signaling Couples Brain Glucose Uptake with Nutrient Availability.* Cell, 2016. **166**(4): p. 867-880.
44. Gratuze, M., et al., *Insulin deprivation induces PP2A inhibition and tau hyperphosphorylation in hTau mice, a model of Alzheimer's disease-like tau pathology.* Sci Rep, 2017. **7**: p. 46359.
45. Wood, H., *Alzheimer disease: Is p-tau the missing link between insulin resistance and AD?* Nat Rev Neurol, 2017. **13**(12): p. 706.
46. Han, X., et al., *Insulin Attenuates Beta-Amyloid-Associated Insulin/Akt/EAAT Signaling Perturbations in Human Astrocytes.* Cell Mol Neurobiol, 2016. **36**(6): p. 851-864.
47. Takano, K., et al., *Insulin expression in cultured astrocytes and the decrease by amyloid β.* Neurochem Int, 2018. **119**: p. 171-177.
48. Rodriguez-Rodriguez, P., et al., *Tau hyperphosphorylation induces oligomeric insulin accumulation and insulin resistance in neurons.* Brain, 2017. **140**(12): p. 3269-3285.
49. Sze, C.I., et al., *Selective regional loss of exocytotic presynaptic vesicle proteins in Alzheimer's disease brains.* J Neurol Sci, 2000. **175**(2): p. 81-90.
50. Yang, Y., et al., *Amyloid-β Oligomers May Impair SNARE-Mediated Exocytosis by Direct Binding to Syntaxin 1a.* Cell Rep, 2015. **12**(8): p. 1244-51.
51. Pham, C., et al., *Astrocytes respond to a neurotoxic Aβ fragment with state-dependent Ca(2+) alteration and multiphasic transmitter release.* Acta Neuropathol Commun, 2021. **9**(1): p. 44.
52. Jourdain, P., et al., *Glutamate exocytosis from astrocytes controls synaptic strength.* Nat Neurosci, 2007. **10**(3): p. 331-9.
53. Pascoal, T.A., et al., *Microglial activation and tau propagate jointly across Braak stages.* Nat Med, 2021. **27**(9): p. 1592-1599.
54. Pickett, E.K., et al., *Amyloid Beta and Tau Cooperate to Cause Reversible Behavioral and Transcriptional Deficits in a Model of Alzheimer's Disease.* Cell Rep, 2019. **29**(11): p. 3592-3604.e5.
55. Laurent, C., et al., *Hippocampal T cell infiltration promotes neuroinflammation and cognitive decline in a mouse model of tauopathy.* Brain, 2017. **140**(1): p. 184-200.

56. Garwood, C.J., et al., *Astrocytes are important mediators of Aβ-induced neurotoxicity and tau phosphorylation in primary culture.* Cell Death Dis, 2011. **2**(6): p. e167.
57. Lian, H., et al., *NFκB-activated astroglial release of complement C3 compromises neuronal morphology and function associated with Alzheimer's disease.* Neuron, 2015. **85**(1): p. 101-115.
58. Zhao, J., T. O'Connor, and R. Vassar, *The contribution of activated astrocytes to Aβ production: implications for Alzheimer's disease pathogenesis.* J Neuroinflammation, 2011. **8**: p. 150.
59. Choi, S.S., et al., *Human astrocytes: secretome profiles of cytokines and chemokines.* PLoS One, 2014. **9**(4): p. e92325.

Tables

Table 1. Demographic information

	CU (N=39)	CI (N=51)
Demographics		
Age, years, mean (SD)	71.7 (6.07)	71.5 (5.92)
Sex, female, n (%)	21 (53.8%)	19 (37.3%)
Education, years, mean (SD)	16.7 (2.34)	16.2 (3.04)
Baseline MMSE score, mean (SD)	29.4 (0.72)	26.3 (4.33)
APOE ε4 carriers, n (%)	15 (38.5%)	22 (43.1%)
Biomarkers		
[^{18}F]-florbetapir global SUVr, mean (SD)	1.11 (0.158)	1.19 (0.200)
Aβ-PET-positive, n (%)	14 (35.9%)	30 (58.8%)
[^{18}F]-flortaucipir temporal meta-ROI SUVr, mean (SD)	1.19 (0.092)	1.29 (0.233)
Tau-PET-positive, n (%)	10 (25.6%)	26 (51.0%)
Plasma GFAP, pg/mL, mean (SD)	145 (59.2)	154 (79.5)

Figure Legends

Figure 1. Associations of plasma glial fibrillary acidic protein with Aβ and Tau-PET. Association between plasma GFAP and **(A)** Aβ-PET ([^{18}F]AV45) and **(C)** Tau-PET ([^{18}F]AV1451). Association of plasma GFAP and with Aβ- and Tau-PET stratified by **(B)** Aβ and **(D)** tau positivity (n = 90).

Figure 2. Gene expression analysis in hippocampal astrocytes from AD mouse models. **(A)** Volcano plots depicting differentially expressed genes (DEGs) in PS2APP (left) or Tau P301S (right) versus WT astrocytes. Insert shows a pie chart of upregulated and downregulated DEG counts. **(B)** Heatmaps with hierarchical clustering depicting DEGs differentiating PS2APP (left) or Tau P301S (right) versus WT astrocytes. **(C)** Venn diagram showing DEGs in each model and the matched genes altered in both.

Figure 3. Protein-protein interaction (PPI) networks in PS2APP and Tau P301S astrocytes. PPI network of **(A)** PS2APP and **(C)** Tau P301S mapping functional categories of genes observed in enriched Gene Ontology biological processes (GOBP). "NA" denotes genes not observed in any enriched GOBPs. Combined score mapped to edges represents the combined confidence interaction scores provided by the STRING database for each pair of genes (values >0.7 are considered high confidence scores). Circos plots showing the connections between functional categories in **(B)** PS2APP and **(D)** Tau P301S PPI.

Figure 4. Gene Ontology network for biological processes (BP), cellular component (CC) and molecular function (MF). Gene Ontology (GO) term network of **(A)** PS2APP and **(D)** Tau P301S constructed using the proportion of overlapping genes between GO terms (Jaccard Coefficient > 0.15) as edges. Radial plots of 10 top GOBP terms ranked from the network by enrichment significance for **(B)** PS2APP and **(E)** Tau P301S. Radial plots of 10 top GO terms ranked from the network by connectivity (degree) for **(C)** PS2APP and **(F)** Tau P301S. Inner circle's bar size maps significance of GO term enrichment and color maps the overall direction (upregulation or downregulation) of the term's group of genes.

Supplemental Figure 1. Correlation between GFAP and other AD biomarkers.
Pairwise correlation matrix between GFAP and seven other known AD biomarkers. Pearson correlation was applied and FDR-adjusted ($\alpha = 0.05$). The strength and direction of the correlation is represented by the color gradient in the upper triangle of the matrix.

Coefficients (black) and adjusted p-values (gray) of the pairwise correlations are shown in the lower triangle.

Supplemental Figure 2. Regulation state of PS2APP and Tau P301S PPI astrocyte networks. Protein-protein interaction networks mapping regulatory states (up/down regulation) of differentially expressed genes in **(A)** PS2APP and **(B)** Tau P301S astrocytes. Combined score mapped to edges represents the combined confidence interaction scores provided by the STRING database for each pair of genes (values > 0.7 are considered high confidence scores).

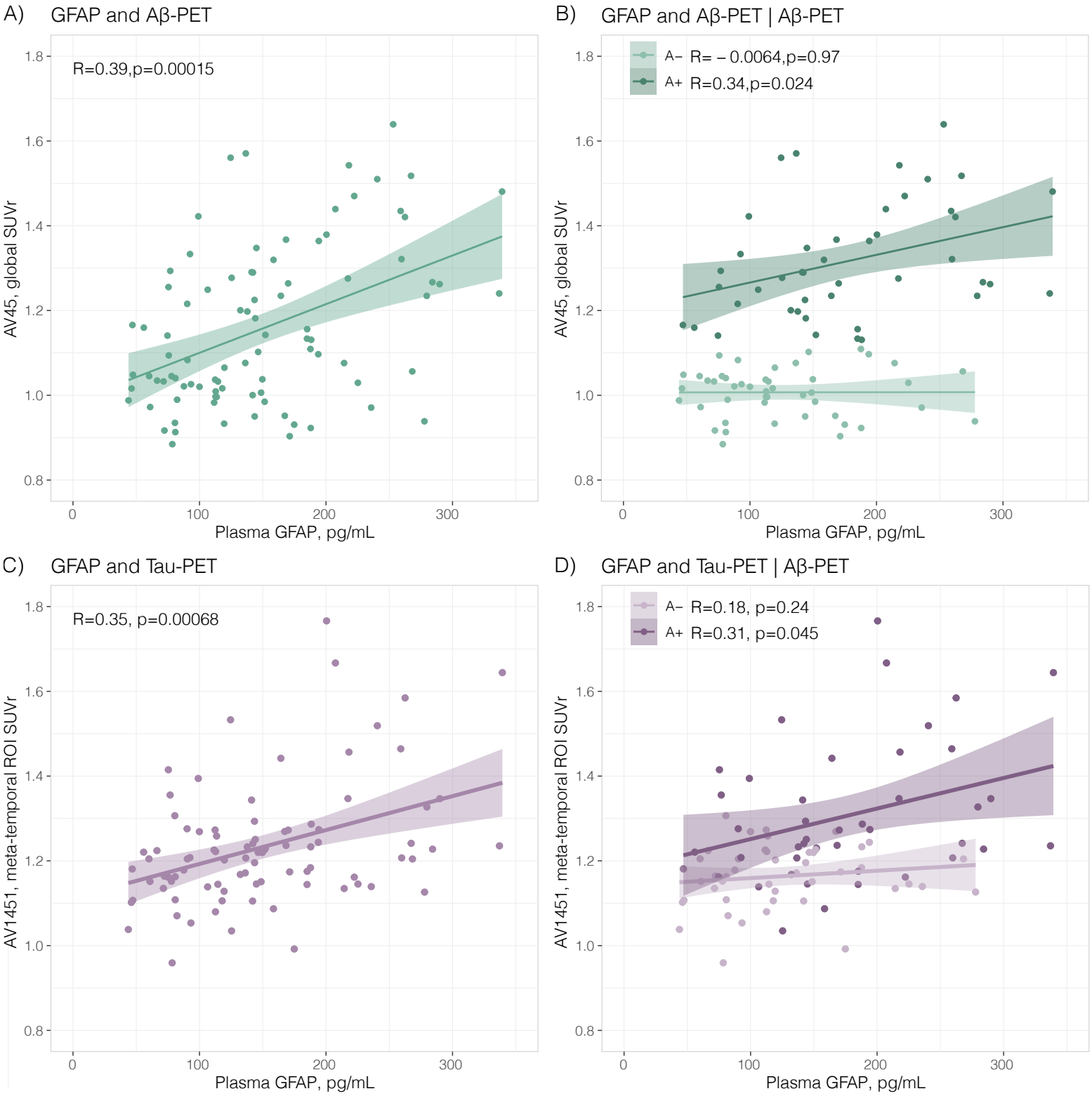
A)
GFAP and Aβ-PET
R=0.39,p=0.00015
AV45, global SUVr
Plasma GFAP, pg/mL
B)
GFAP and Aβ-PET | Aβ-PET
A− R= − 0.0064,p=0.97
A+ R=0.34,p=0.024
AV45, global SUVr
Plasma GFAP, pg/mL
C)
GFAP and Tau-PET
R=0.35, p=0.00068
AV1451, meta-temporal ROI SUVr
Plasma GFAP, pg/mL
D)
GFAP and Tau-PET | Aβ-PET
A− R=0.18, p=0.24
A+ R=0.31, p=0.045
AV1451, meta-temporal ROI SUVr
Plasma GFAP, pg/mL

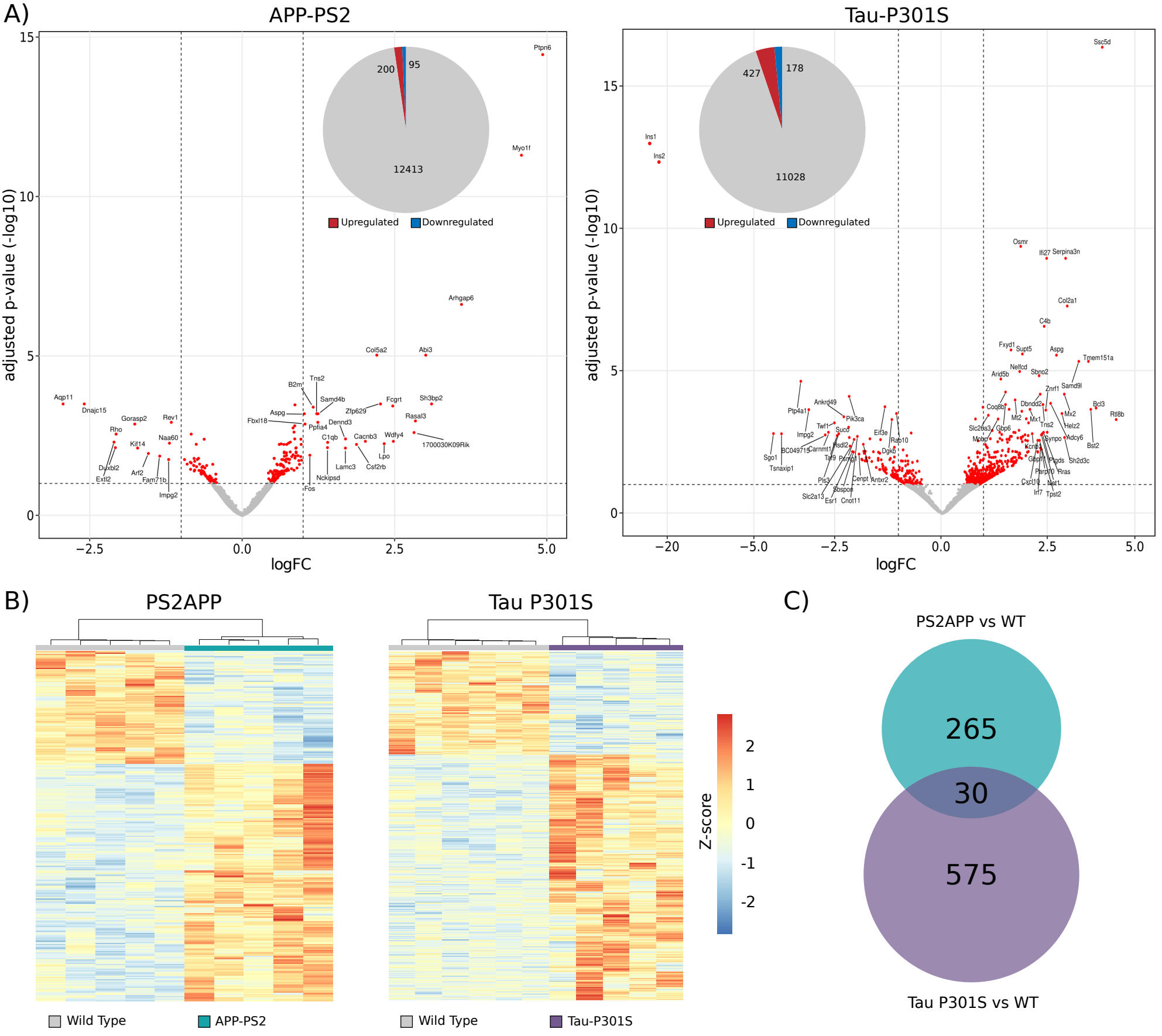
A)
APP-PS2
Tau-P301S
adjusted p-value (-log10)
logFC
Upregulated
Downregulated
200
95
12413
427
178
11028
B)
PS2APP
Tau P301S
Z-score
Wild Type
APP-PS2
Wild Type
Tau-P301S
C)
PS2APP vs WT
265
30
575
Tau P301S vs WT

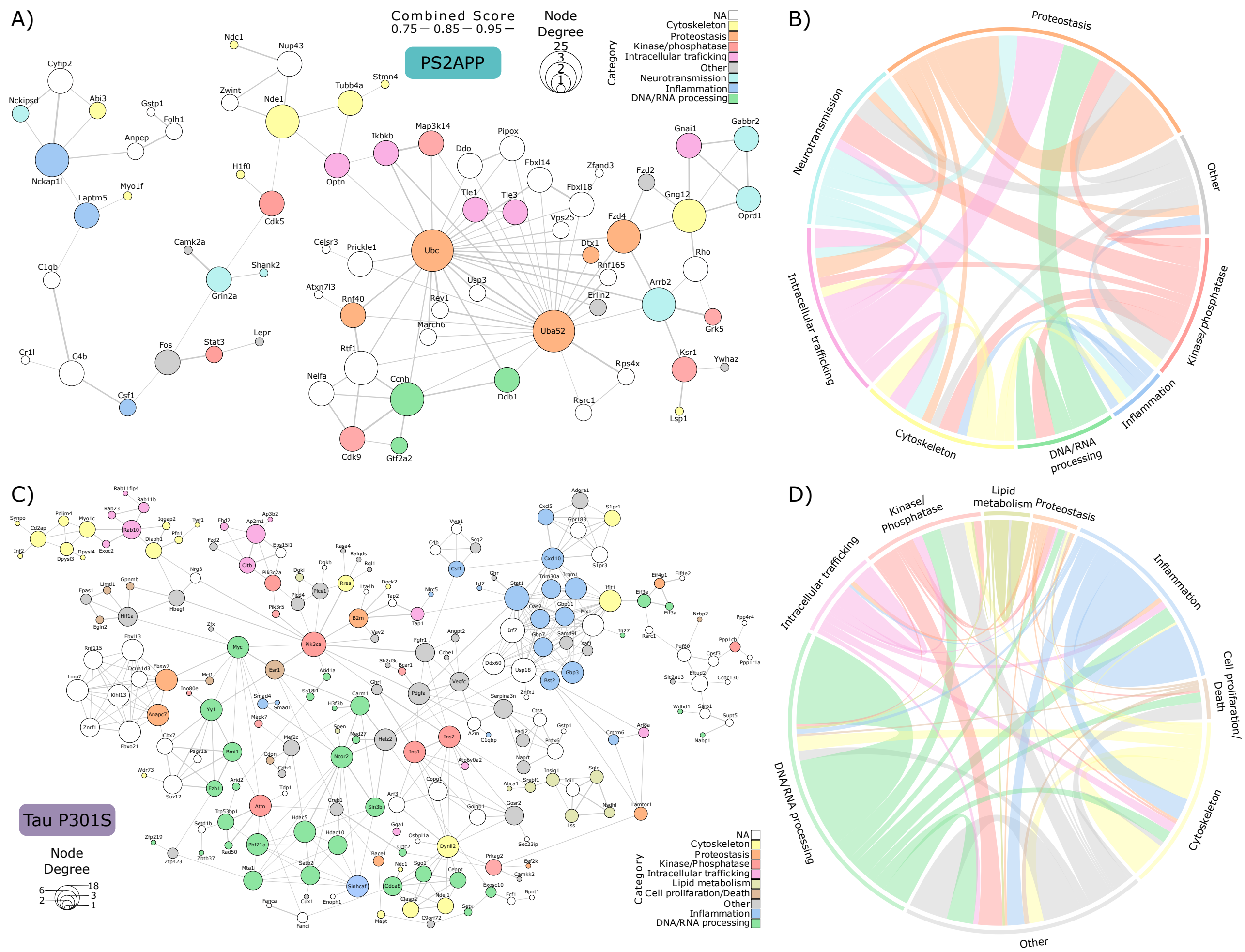
A)
Combined Score
0.75 — 0.85 — 0.95 —
PS2APP
Node Degree
25
3
2
1
Category
NA
Cytoskeleton
Proteostasis
Kinase/phosphatase
Intracellular trafficking
Other
Neurotransmission
Inflammation
DNA/RNA processing
B)
Proteostasis
Other
Kinase/phosphatase
Inflammation
DNA/RNA processing
Cytoskeleton
Intracellular trafficking
Neurotransmission
C)
Tau P301S
Node Degree
18
6
3
2
1
Category
NA
Cytoskeleton
Proteostasis
Kinase/Phosphatase
Intracellular trafficking
Lipid metabolism
Cell prolifaration/Death
Other
Inflammation
DNA/RNA processing
D)
Kinase/ Phosphatase
Lipid metabolism
Proteostasis
Inflammation
Cell prolifaration/ Death
Cytoskeleton
Other
DNA/RNA processing
Intracellular trafficking

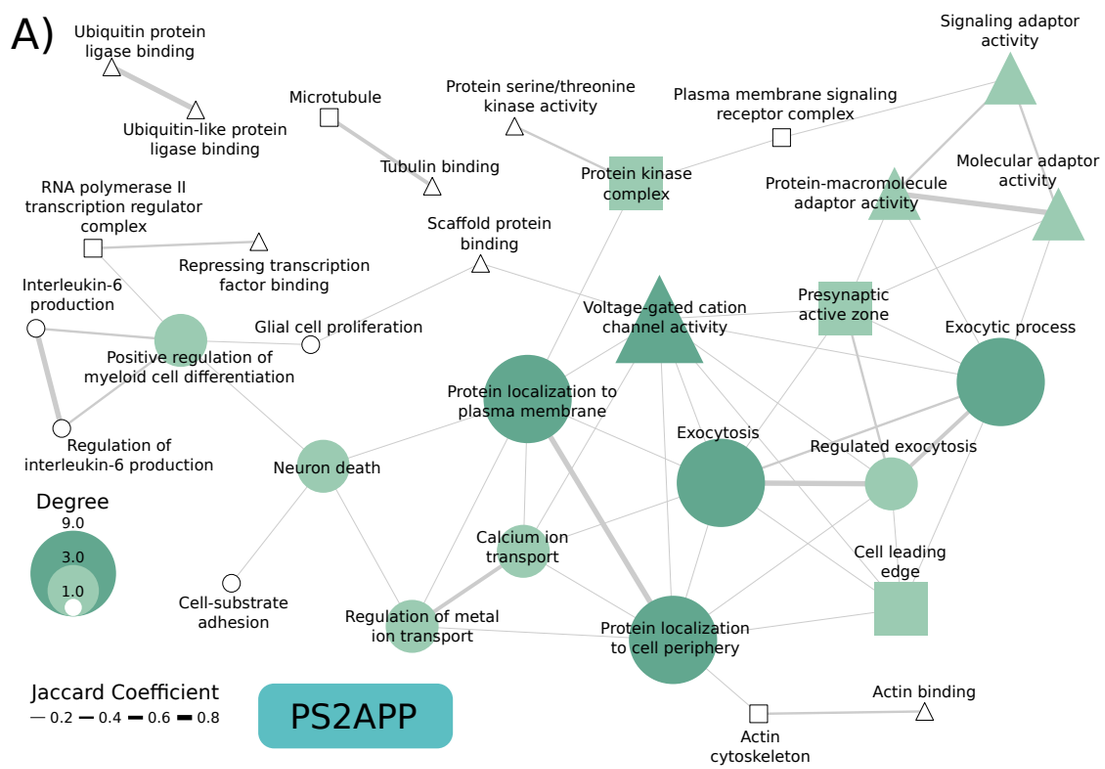

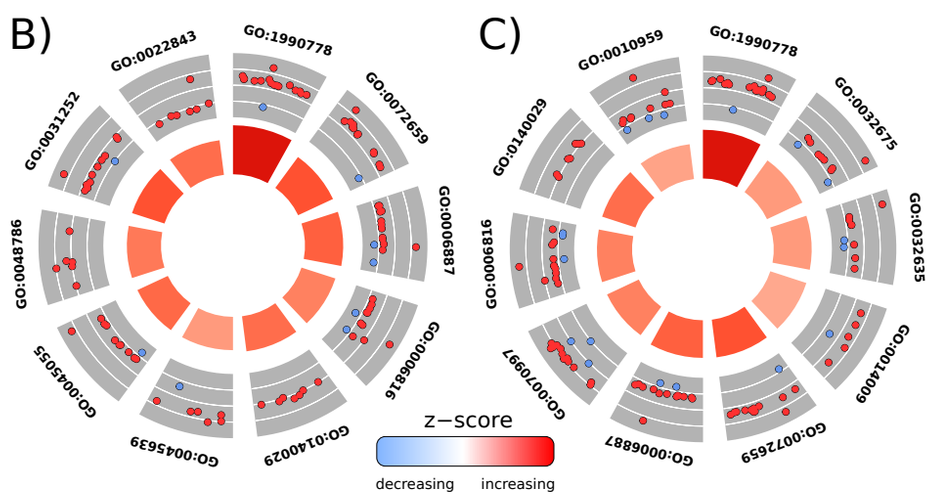

ID	Description
GO:0022843	voltage−gated cation channel activity
GO:0006887	exocytosis
GO:1990778	protein localization to cell periphery
GO:0072659	protein localization to plasma membrane
GO:0140029	exocytic process
GO:0045639	positive regulation of myeloid cell differentiation
GO:0045055	regulated exocytosis
GO:0048786	presynaptic active zone
GO:0006816	calcium ion transport
GO:0031252	cell leading edge

ID	Description
GO:1990778	protein localization to cell periphery
GO:0032675	regulation of interleukin−6 production
GO:0032635	interleukin−6 production
GO:0014009	glial cell proliferation
GO:0072659	protein localization to plasma membrane
GO:0006887	exocytosis
GO:0070997	neuron death
GO:0006816	calcium ion transport
GO:0140029	exocytic process
GO:0010959	regulation of metal ion transport

Gene Status (logFC)

downregulated genes upregulated genes

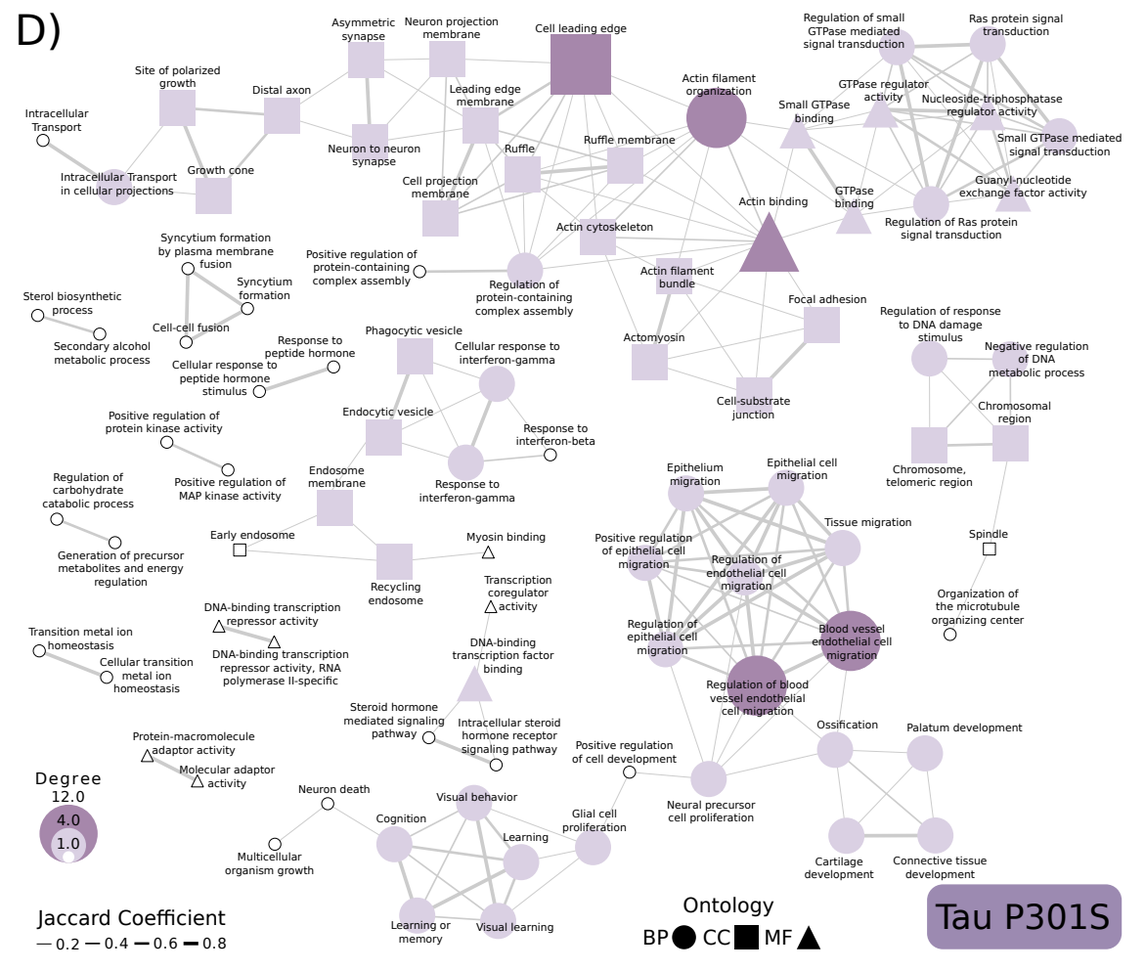

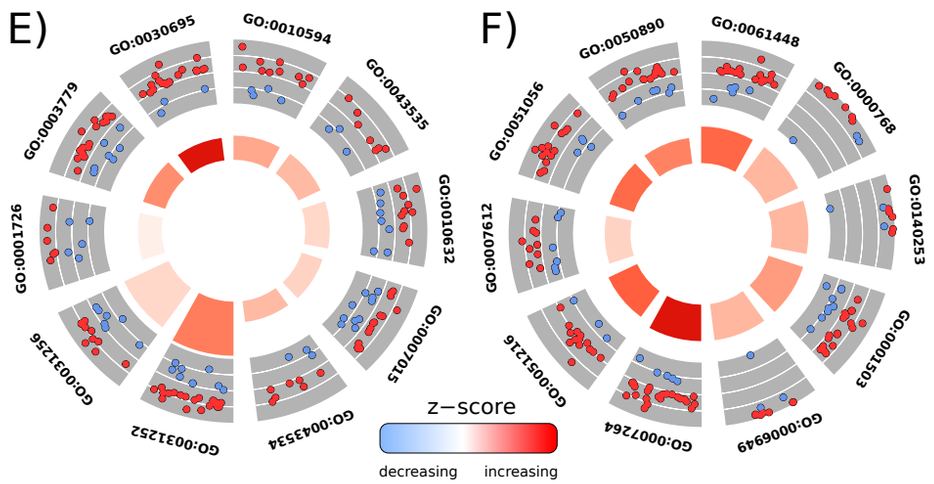

ID	Description
GO:0003779	actin binding
GO:0007015	actin filament organization
GO:0031252	cell leading edge
GO:0043534	blood vessel endothelial cell migration
GO:0043535	regulation of blood vessel endothelial cell migration
GO:0001726	ruffle
GO:0010594	regulation of endothelial cell migration
GO:0010632	regulation of epithelial cell migration
GO:0030695	GTPase regulator activity
GO:0031256	leading edge membrane

ID	Description
GO:0061448	connective tissue development
GO:0000768	syncytium formation by plasma membrane fusion
GO:0140253	cell−cell fusion
GO:0001503	ossification
GO:0006949	syncytium formation
GO:0007264	small GTPase mediated signal transduction
GO:0051216	cartilage development
GO:0007612	learning
GO:0051056	regulation of small GTPase mediated signal transduction
GO:0050890	cognition

Gene Status (logFC)

downregulated genes upregulated genes

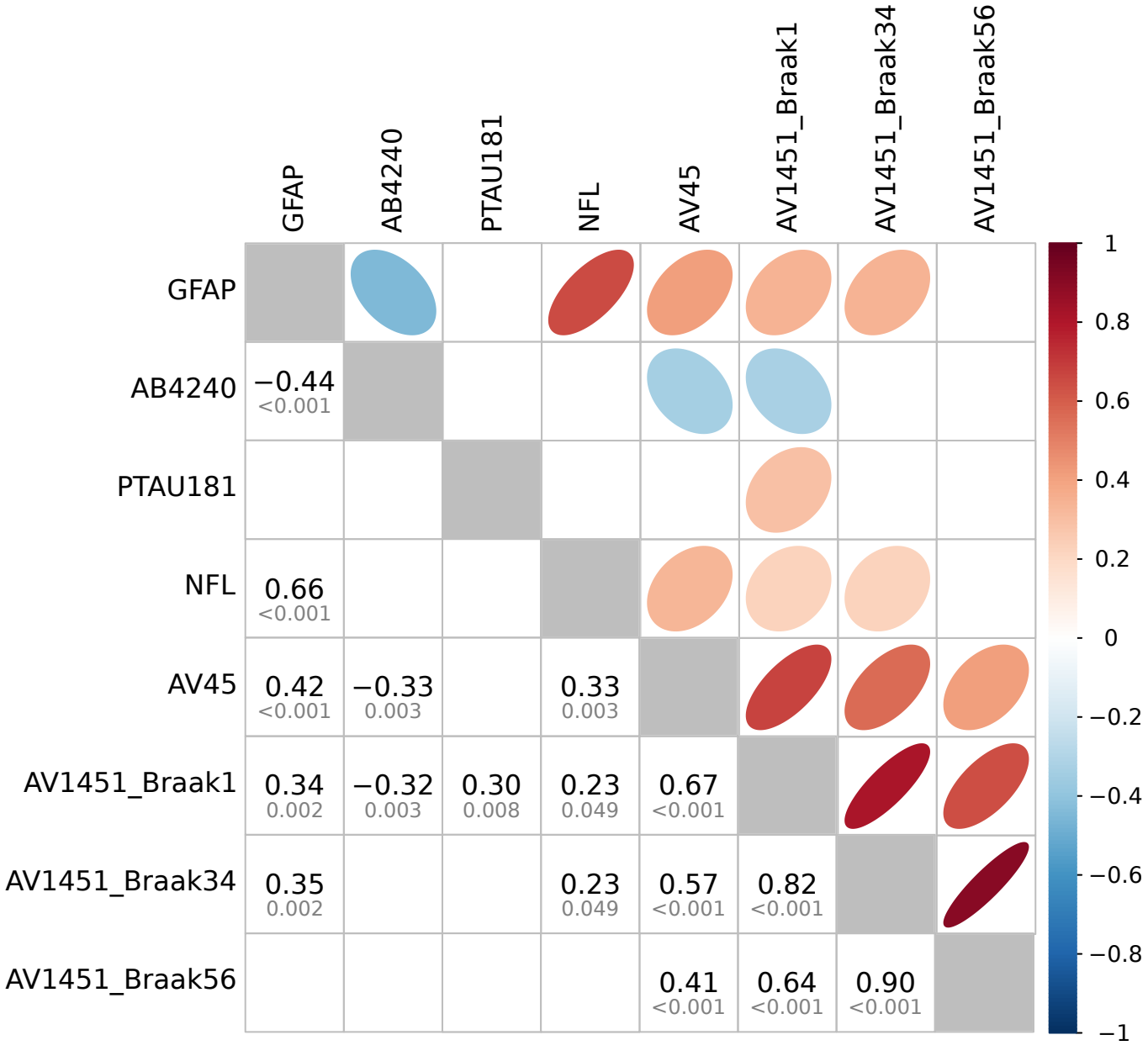
GFAP
AB4240
PTAU181
NFL
AV45
AV1451_Braak1
AV1451_Braak34
AV1451_Braak56
−0.44
<0.001
0.66
<0.001
0.42
<0.001
−0.33
0.003
0.33
0.003
0.34
0.002
−0.32
0.003
0.30
0.008
0.23
0.049
0.67
<0.001
0.35
0.002
0.23
0.049
0.57
<0.001
0.82
<0.001
0.41
<0.001
0.64
<0.001
0.90
<0.001
1
0.8
0.6
0.4
0.2
0
−0.2
−0.4
−0.6
−0.8
−1

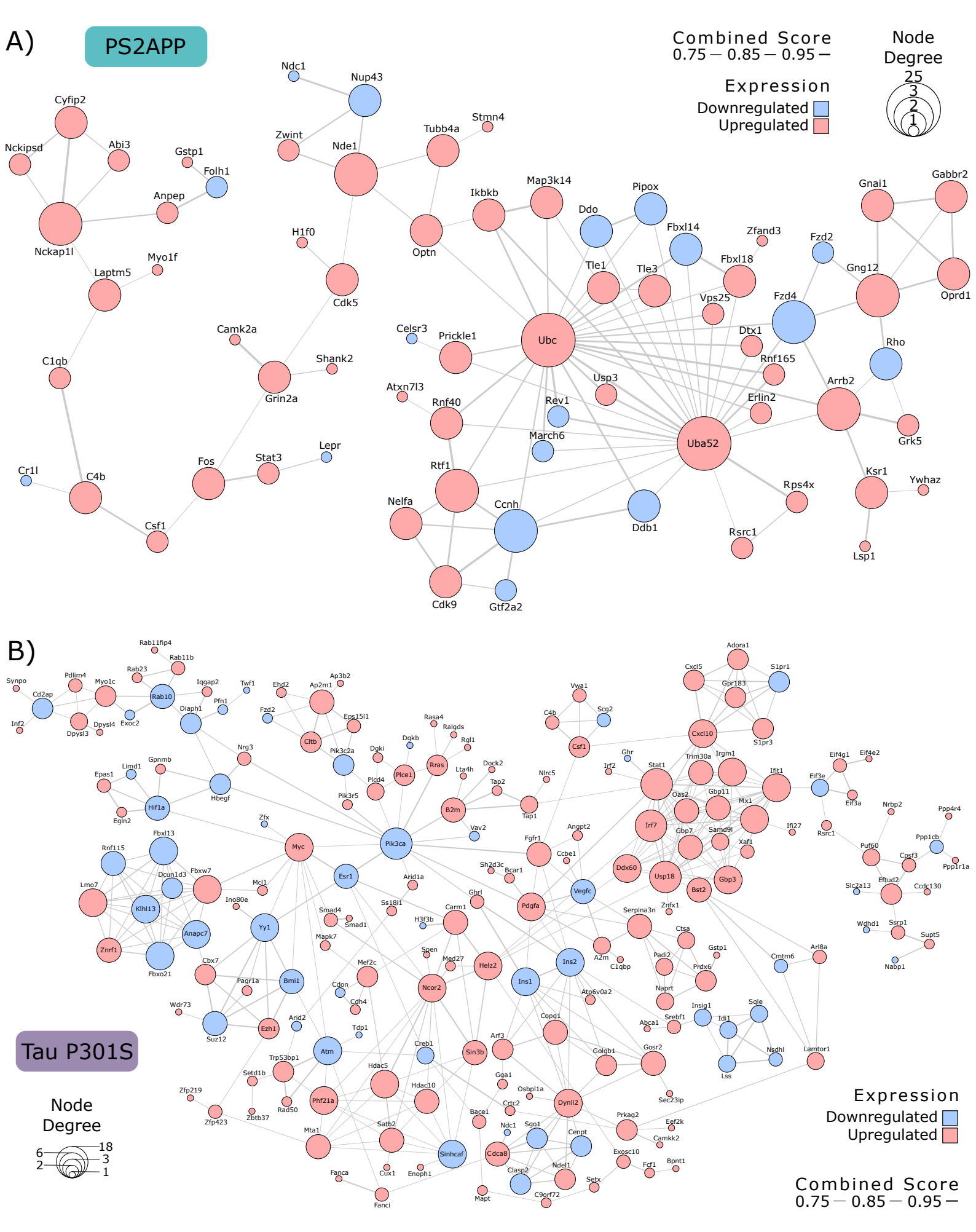
A)
PS2APP
Combined Score
0.75 — 0.85 — 0.95 —
Expression
Downregulated
Upregulated
Node
Degree
25
3
2
1
Ndc1
Nup43
Cyfip2
Nckipsd
Abi3
Gstp1
Folh1
Zwint
Nde1
Tubb4a
Stmn4
Anpep
Nckap1l
Laptm5
Myo1f
H1f0
Cdk5
Optn
Ikbkb
Map3k14
Ddo
Pipox
Fbxl14
Zfand3
Fzd2
Gnai1
Gabbr2
Tle1
Tle3
Fbxl18
Gng12
Oprd1
Vps25
Fzd4
Dtx1
Rho
Camk2a
Shank2
Grin2a
Celsr3
Prickle1
Ubc
Rnf165
Arrb2
Usp3
Atxn7l3
Rnf40
Rev1
Erlin2
Grk5
March6
Uba52
C1qb
Lepr
Stat3
Fos
Cr1l
C4b
Rtf1
Ksr1
Ywhaz
Rps4x
Nelfa
Ccnh
Ddb1
Csf1
Rsrc1
Lsp1
Cdk9
Gtf2a2
B)
Tau P301S
Node
Degree
6
2
18
3
1
Expression
Downregulated
Upregulated
Combined Score
0.75 — 0.85 — 0.95 —
Rab11fip4
Rab11b
Rab23
Synpo
Pdlim4
Myo1c
Iqgap2
Twf1
Ehd2
Ap2m1
Ap3b2
Cd2ap
Rab10
Pfn1
Diaph1
Fzd2
Eps15l1
Inf2
Dpysl3
Dpysl4
Exoc2
Cltb
Rasa4
Ralgds
Dgkb
Rgl1
Dgki
Pik3c2a
Rras
Plce1
Plcd4
Dock2
Lta4h
Tap2
Nlrc5
Tap1
B2m
Pik3r5
Nrg3
Limd1
Gpnmb
Epas1
Hbegf
Hif1a
Egln2
Zfx
Vav2
Pik3ca
Myc
Fbxl13
Rnf115
Dcun1d3
Fbxw7
Lmo7
Klhl13
Mcl1
Ino80e
Esr1
Arid1a
Ss18l1
Smad4
Smad1
Yy1
Anapc7
Znrf1
Fbxo21
Mapk7
Cbx7
Pagr1a
Bmi1
Wdr73
Suz12
Ezh1
Arid2
Tdp1
Atm
Trp53bp1
Setd1b
Zfp219
Zfp423
Zbtb37
Rad50
Phf21a
Mta1
Fanca
Fanci
Cux1
Enoph1
Sinhcaf
Satb2
Hdac5
Hdac10
Cdcd8
Mef2c
Cdon
Cdh4
Spen
Med27
Helz2
Ncor2
Carm1
H3f3b
Ghrl
Pdgfa
Vegfc
Ins2
Ins1
Creb1
Sin3b
Arf3
Copg1
Gga1
Osbpl1a
Crtc2
Dynll2
Bace1
Ndc1
Sgo1
Cenpt
Clasp2
Ndel1
Setx
C9orf72
Mapt
Prkag2
Eef2k
Camkk2
Exosc10
Fcf1
Bpnt1
Sec23ip
Golgb1
Gosr2
Nsdhl
Lamtor1
Lss
Insig1
Idi1
Sqle
Abca1
Srebf1
Naprt
Atp6v0a2
Padi2
Prdx6
Gstp1
Cmtm6
Arl8a
Nabp1
A2m
C1qbp
Serpina3n
Znfx1
Ctsa
Wdhd1
Ssrp1
Supt5
Slc2a13
Eftud2
Ccdc130
Puf60
Cpsf3
Ppp1cb
Ppp1r1a
Nrbp2
Ppp4r4
Rsrc1
Ifi27
Xaf1
Gbp3
Bst2
Ddx60
Usp18
Irf7
Gbp7
Samd9l
Oas2
Gbp11
Mx1
Stat1
Trim30a
Irgm1
Ifit1
Eif3e
Eif3a
Eif4g1
Eif4e2
Irf2
Ghr
Nlrc5
Ccbe1
Fgfr1
Angpt2
Sh2d3c
Bcar1
Vwa1
Scg2
C4b
Csf1
Cxcl10
Cxcl5
Gpr183
S1pr1
S1pr3
Adora1